IEEE Access
Multidisciplinary | Rapid Review | Open Access Journal

Received 4 June 2025, accepted 25 June 2025, date of publication 27 June 2025, date of current version 7 July 2025.

Digital Object Identifier 10.1109/ACCESS.2025.3583915

RESEARCH ARTICLE

Revolutionary Unconventional Transmission Line Designs With Higher Line Loadability

MUSHFIQUL ABEDIN KHAN, (Graduate Student Member, IEEE), AND MONA GHASSEMI, (Senior Member, IEEE)

Department of Electrical and Computer Engineering, Zero Emission, Realization of Optimized Energy Systems (ZEROES) Laboratory, The University of Texas at Dallas, Richardson, TX 75080, USA

Corresponding author: Mona Ghassemi (mona.ghassemi@utdallas.edu)

This work was supported in part by the National Science Foundation under Award 2306098.

ABSTRACT Traditionally, overhead AC transmission lines have been used to transfer electrical power from the generation to the distribution sector. The capacitance and inductance of these lines are significantly influenced by the size and arrangement of the subconductors in each phase, which in turn affects the transmission capacity. Conventional transmission lines typically employ a circular symmetry for the arrangement of subconductors in each phase. However, by altering the number and placement of these subconductors, the power transfer capacity of the lines can be significantly increased. Unconventional transmission lines leverage this principle by deviating from the traditional circular symmetry, resulting in a lower characteristic or surge impedance (Z_c), which enhances the surge impedance loading (SIL). This paper introduces new designs for unconventional transmission lines, optimized under strict criteria to minimize corona discharge effects while maintaining a narrow corridor width (CW). Compared to a conventional transmission line from the literature—with a SIL of 996 MW and a line width of 24.6 meters (yielding a power density of 40.5 MW/m)—our optimally designed conventional HSIL line achieves a SIL of 1351 MW (a 36% increase) and a line width of only 8.4 meters (a 66% reduction), resulting in a power density of 160.8 MW/m (a 297% increase). Even greater improvements are observed with unconventional HSIL designs, reaching a SIL of 1592 MW—representing a 60% increase over the conventional line and an 18% improvement over the best conventional HSIL design. These findings offer promising prospects for the future of modern transmission networks.

INDEX TERMS Surge impedance loading, transmission lines, subconductors, line design.

I. INTRODUCTION

The electric power industry has undergone significant advancements in recent years, particularly in power generation and distribution. Notable developments include the shift from large synchronous generators to smaller, more efficient machines and the increasing integration of renewable energy sources into the grid. The generation and distribution sectors are linked by extra-high voltage (EHV) AC transmission systems, which can be either overhead lines or underground cables. However, EHV AC underground cables can be up to ten times more expensive than overhead lines at the same voltage level. Additionally, these cables exhibit high capacitance, resulting in excessive charging currents that limit their practical length. Among line constraints, especially at EHV levels, bus voltage drops play a key role in today's heavily loaded grids. To mitigate these challenges, reactive compensation techniques such as series capacitors, shunt capacitors/reactors, and flexible AC transmission systems (FACTS) are often employed. However, these solutions can be costly and require complex protection and management strategies [1].

Achieving net-zero emissions in the US will require a major expansion of the high-voltage transmission network to accommodate large-scale renewable energy integration. Estimates indicate that by 2030 and 2050, approximately 300 GW and 1.5 TW of power must be supplied by solar and

The associate editor coordinating the review of this manuscript and approving it for publication was Diego Bellan.

wind energy, respectively. This transition necessitates a 60% increase in the transmission capacity by 2030 and a threefold expansion by 2050, with costs projected up to $360 billion and $2.4 trillion, respectively [2]. However, constructing new transmission lines is a complex process, often delayed by lengthy approval times, legal right-of-way (ROW) challenges, and high associated costs – often exceeding the cost of the lines themselves [1]. For instance, building a 500 kV overhead transmission line in the US costs between $4.5 million and $5.1 million per mile, depending on the state [3].

Given these challenges, transmission expansion planning (TEP) strategies that use fewer transmission lines while enhancing their power transfer capability are highly desirable [4], [5], [6]. Research on unconventional high surge impedance loading (HSIL) lines suggests that they can significantly reduce costs by minimizing the number of lines required while maintaining power delivery efficiency [7]. To our knowledge, G. N. Alexandrov was the first to propose non-circular conductor bundle arrangements to enhance the natural power [8], [9], [10], [11], an approach later explored by various researchers [12], [13], [14], [15], [16], [17], [18], [19]. Increases in SIL or natural power can be achieved by

- Increasing the number of subconductors per bundle,
- Expanding the bundle radius,
- Reducing the phase-to-phase distance, among other design modifications.

The above constraints are all seen in this paper. Specifically, to achieve the latter two, the conventional circular symmetry of the phase bundles can be broken, to result in a higher bundle radius for the outer phases, while also bringing the phases closer together. Additionally, to account for this change in symmetry of the circular bundled conductors, the individual phases must also undergo subconductor transposition. These adjustments effectively reduce the line inductance while increasing the line capacitance, leading to a lower surge or characteristic impedance (Z_c), and consequently reducing the need for reactive power compensation.

This paper presents new, optimized, 500 kV unconventional lines. Suitable conductor selection is made based on weight and cost-effectiveness. The term ''unconventional'' refers to the asymmetrical positioning of the bundled subconductors. The design process incorporates key constraints including the maximum allowable electric field on the conductor surface, minimum phase spacing, and conductor height restrictions. The proposed designs ensure compliance with electrical limitations while maintaining practical feasibility. The results demonstrate that the new HSIL lines achieve significantly higher SIL compared to the conventional transmission lines.

II. METHOD

A. BACKGROUND

The natural power of a transmission line depends on its phase voltage, $V_\phi$and characteristic impedance, Z_c, and is given by $P_n{=}3V_\phi^2\big/Z_c$. Z_c is found by the square root of the ratio of the inductance, L to the capacitance, C of these lines. L and C are directly dependent on the number and position of the bundled subconductors. As known, in conventional lines with a single conductor in each phase $L = 2{\times}10^{-7}\ln\left(\sqrt[3]{D_{12}D_{23}D_{31}}\big/GMR\right)$, where GMR is the geometric mean radius, and $D_{ij}(i, j = 1, 2, 3\ and\ i \neq j)$ is the distance between phases i and j. The geometric mean radius, GMR, is the effective radius of the conductors, after considering the skin effect. For ACSR conductors, the usual conductor type used in EHV lines, the amount of GMR is provided by manufacturers, given on the datasheet of the conductor. Similarly, $C = 2\pi\epsilon\big/ln\left(\sqrt[3]{D_{12}D_{23}D_{31}}\big/r\right)$, where ϵ is the permittivity of free space and r is the radius of the conductor [1]. When calculating L, the GMR of a bundle conductor configuration where we have more than one conductor in each phase, and conductors, now called subconductors, are located on a circle symmetrically, is given by $GMR_b{=}\left[N \times GMR{\times}\ (A)^{N-1}\right]^{1/N}$, where N is the number of subconductors of the bundle conductor on a circle of radius A. Likewise, to calculate C for a line with a bundle conductor, r will be $r_b{=}\left[N \times r{\times}\ (A)^{N-1}\right]^{1/N}$. The geometric mean distance, $GMD = \sqrt[3]{D_{12}D_{23}D_{31}}$, on the other hand, is the average distance between the phases. For the bundle conductor, GMD is indeed the average distance between the bundle centers of phases. Increasing the GMR and reducing the GMD leads to an increase in C and a decrease in L, thus causing the surge impedance or characteristic impedance to decrease. This means that an increase in SIL. The conventional towers have grounded steel portions between phases, resulting in the distance between the phases essentially being equal to the sum of two phase-to-ground distances. Removal of these grounded tower portions can help significantly reduce phase-to-phase distances, GMD, and in turn the corridor width (CW), which again, in turn, helps in cost reduction, and increases the power density of the transmission lines. Increasing the bundle circle radius and using a larger number of subconductors in the bundle can lead to an increase in GMR_b and r_b, and in turn, increasing SIL. Using the aforementioned techniques leads to line designs known as high surge impedance load (HSIL) lines. In this paper, we call these lines conventional HSIL lines, since we are considering adding another technique where we break the circular bundle symmetry, and we call these lines unconventional HSIL lines. We show that the unconventional HSIL lines can achieve higher natural power or SIL. To enhance the SIL, we have also increased the number of subconductors, N per phase. To maintain cost efficiency, the chosen conductor's cross-sectional area must be less than the conventional one.

B. DESIGN OF UNCONVENTIONAL LINES

The primary step in designing any transmission line is to set the constraints. One of the most important constraints to meet when designing a transmission line is to keep the electric field on the surface of the subconductors, E_{max} below a certain threshold, E_{th}, which comes from the corona onset

voltage. Corona discharge happens under high voltage stress on subconductors, which can be a common event in transmission lines. This can lead to power loss, audible noise (AN), and electromagnetic interferences including radio interference (RI) and television interference (TVI). Setting E_{th} to 20 kV/cm would help minimize these effects [20]. This must be maintained for each of the phases, $i \in \{1, 2, 3\}$ as shown in Eq. (1). The interphase gap, D_{ij}^{p2p}, and the distance of each phase from the ground, H_i^{p2g}, must also be greater than their respective threshold values as shown in Eqs. (2) and (3).

$$E_i^{max} < E_{th}, \quad i \in \{1, 2, 3\} \tag{1}$$

$$D_{ij}^{p2p} > D_{min,p2p}, \quad i, j \in \{1, 2, 3\} \quad \& i \neq j \tag{2}$$

$$H_i^{p2g} > H_{min,p2g}, \quad i \in \{1, 2, 3\} \tag{3}$$

$D_{min,p2p}$ was chosen to be 6.7 m as found in an existing 500 kV compact line [14]. Additionally, $H_{min,p2g}$ was taken as 21 m, a little more than 6.7 m below the average height of 28 m of the conventional 500 kV line found in the literature [14]. An increase in *SIL* due to a reduction in Z_c readily means that there is a difference in the maximum conductor surface electric field, E_{max}. This directly impacts the effect of corona discharge in the system, from corona power loss to electromagnetic interferences (EMIs). This issue is given top priority, and it is ensured that the newly designed line meets the E_{max} constraint that keeps these effects within acceptable limits through Eq. (1). Eq (2) says that the minimum phase gap must be greater than 6.7 m as shown in [14]. This constraint must be met as this minimum distance is based on the lightning and switching overvoltages [1]. The minimum conductor-to-ground distance on the other hand has been set considering the sag at midspan. Thus, meeting this constraint is also crucial. Ensuring a minimum phase-to-phase distance and minimum height of the conductors also align with the constraint in (1).

The next step is to select a suitable conductor. As found in [21], recently, 500 kV transmission lines have been 2 subconductors per bundle consisted of ACSR conductors of size around 2032 and 2036 kcmil. Taking this as the reference, depending on the number of subconductors per bundle, N, a conductor size is first selected. Next, the overall ampacity, cost, and weight are analyzed and compared to those of the standard, and the one for which all parameters fit this comparison is then chosen for line design. In this paper, we have shown designs with $N = 2$ to 4. For $N = 2$, we have selected 2 Mockingbird conductors, each having a size of 2034.5 kcmil, which complies with the references mentioned above, for the base case, which has a conventional design. The outer diameter of Mockingbird is 1.6670 inches, its weight is 2158 lb/kft, and its ampacity is 1550 A.

For optimal designs, later shown in Figs. 4, 5, and 8, with $N = 2$, Bluebird conductor is chosen, which is similar in size (2156 kcmil) to the base case; the total cost per conductor per 1000 ft is \$4,569 (for material)+\$6,613 (for installation)+\$277 (for accessories)=\$11,459 [3]; therefore, for $N = 2$, it will be 2×\$11,459=\$22,918. For $N = 2$, the total weight in pounds per 1000 ft is $2 \times 2510 = 5020$. For $N = 2$, the total ampacity at 75 °C is 3240 A. The considered conductors for $N = 3$, 4, 5, and 6, and their specifications are presented in Table 1. As seen from Table 1, we chose smaller conductors for $N = 3$, 4, 5, and 6, so that the total cost of lines with three to six conductors is less than that for the line with two conductors. This means in terms of conductor cost, the lines with three to six conductors per phase are cheaper than the line with $N = 2$. Moreover, note that the total weight of these lines is also less than that for the line with two conductors, meaning in terms of tower and foundation costs, those lines with higher numbers of subconductors per phase are not more expensive. Also, as shown later in this paper, the optimal designs presented in this paper have a narrower line width, and in turn, narrower ROW compared to the base design. Therefore, considering all factors, the optimally designed lines in this paper are cheaper than the base design. Furthermore, note that we chose the conductor types in a way that, besides being cheaper in terms of conductor, tower, and foundation costs, those lines have higher ampacities than the line with two subconductors per phase.

TABLE 1. Details of the considered conductors for the lines [3], [22].

N	Conductor	Outer diameter (in)	Total Ampacity at 75°C	Total Weight (lb/kft)	Total Cost (\$/kft)
2	Bluebird	1.762	2×1620 =3240	2×2510 =5020	22,918
3	Bittern	1.345	3×1165 =3495	3×1432 =4296	17,988
4	Rail	1.165	4×975= 3900	4×1075 =4300	19,196
5	Coot	1.040	5×865= 4325	5×805= 4025	19,940
6	Parakeet	0.914	6×725= 4350	6×714= 4285	21,456

Besides the mentioned parameters, the bundle spacing, B, is another parameter that requires initialization. To start, B is taken as 0.457 m based on existing 500 kV transmission lines [21]. Once the values are selected as outlined above, the subconductors are arranged adjacent to each other, forming horizontally placed phases with conductor bundles that replicate the "circular" geometry of the conventional design. Then, E_i^{max} is calculated for each phase i to verify its compliance with Eq. (1). If this is violated, D_{ij}^{p2p} is increased in small increments and E_i^{max} is recalculated iteratively until the first constraint is satisfied. Once achieved, one subconductor from each of the outer phases, A_1 and C_1, are fixed in place, while the remaining subconductors are adjusted along arcs of increasing radii centered at the fixed subconductors, ensuring all constraints are maintained. The design that yields the highest surge impedance loading (SIL) is identified as the optimal configuration.

C. ELECTRIC FIELD CALCULATION

Accurate evaluation of the electric field on the surface of the subconductors during line design is crucial, as this is

one of the primary constraints required to be met. Maxwell's Potential coefficients, $[P]$, are found, followed by setting $[P][q] = [V]$, where $[q]$ represents the stored charge and $[V]$ shows the potential of each conductor. The elements of $[P]$ are found as shown in [20]:

$$P_{mm} = \frac{1}{2\pi\epsilon_0} \ln \frac{2H_m}{r_m} \tag{4}$$

$$P_{mn} = \frac{1}{2\pi\epsilon_0} \ln \sqrt{1 + 4\frac{H_m H_n}{D_{mn}^2}} \tag{5}$$

where r_m and H_m are the radius and the average height of the subconductor m in a phase, respectively, and D_{mn} is the gap between subconductors m and n. Having $[q]$, the electric field on subconductors of each phase can be calculated by ignoring the effect of subconductors from other phases and also ignoring the earth effect, using $E = \left(q/2\pi\epsilon_0\right)\left(1/r\right)\left[1 + (N-1)\,r/R\right]$, where it is assumed the subconductors are located on a circle with a radius of R symmetrically. In conventional lines, since the distances from subconductors from other phases and the image subconductors to the subconductors in the phase we are calculating the electric stress on its subconductors are much greater than the distances between subconductors in that phase, the above assumptions are valid. However those assumptions are not valid for unconventional HSIL lines, and we need to consider all those effects. Therefore, we need to develop a new approach for calculating the electric field intensity of subconductors of unconventional HSIL lines. For this reason, we have developed a model described in one of our other papers [23], where each subconductor with radius, r, is modeled using n_m line charges. Fig. 1 shows the hypothetical line charges which are placed around an imaginary cylinder with a radius of $r/2$ centered on the axis of the subconductor. The electric potential at the points on the surface of the conductor marked with P are found using:

$$E\,(p) = \frac{1}{2\pi\,\varepsilon_0} \sum_{i=1}^{nxn_m} \frac{q_i}{\left|\overrightarrow{r_p} - \overrightarrow{r_i}\right|^2} \left(\overrightarrow{r_p} - \overrightarrow{r_i}\right) \tag{6}$$

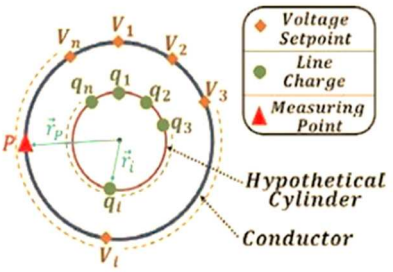

FIGURE 1. Modeling of subconductors with n_m line charges [23].

where, q_i is the charge on the i^{th} line charge, n is the number of subconductors, and r_p and r_i are the radius of the conductor and the radius of the inner hypothetical cylinder, respectively as seen in [23]. This model leads to very accurate results for electric field calculations as verified by using COMSOL Multiphysics [23].

D. TRANSPOSITION

As mentioned earlier, Z_c is dependent on L and C of the line. To keep these consistent throughout in unconventional lines, transposition must be considered. The unconventional lines are designed with minimum adjacent phase spacing while also maintaining $E_i^{max} < E_{th}$. For this reason, we have to transpose the bundle arrangement besides phase transposition. In conventional lines, we have transposition for phases only since the bundle configuration is identical in the three phases. However, this is not the case for unconventional HSIL lines, where subconductor arrangements are different in different phases. As shown in Fig. 2, the line must be transposed in two locations to ensure that each phase covers each position for one-third of the line length. For unconventional HSIL lines, we also have bundle transposition in the two locations mentioned above.

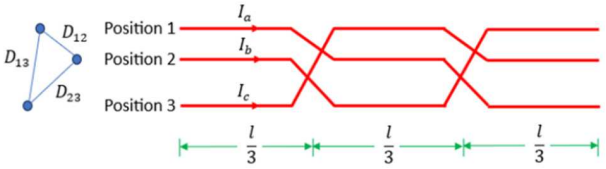

FIGURE 2. A completely transposed three-phase line.

The conductor locations are labeled as 1, 2, and 3, with distances D_{12}, D_{23}, and, D_{13} between them. To calculate the inductance of this transmission line, we assume balanced positive-sequence currents that satisfy the condition:

$$I_A + I_B + I_C = 0 \tag{7}$$

The total flux linking phase A while it occupies positions 1, 2, and 3 is then determined accordingly.

$$\lambda_{A1} = 2 \times 10^{-7}\left[I_A \ln \frac{1}{D_{s1}} + I_B \ln \frac{1}{D_{12}} + I_C \ln \frac{1}{D_{31}}\right] \tag{8}$$

$$\lambda_{A2} = 2 \times 10^{-7}\left[I_A \ln \frac{1}{D_{s2}} + I_B \ln \frac{1}{D_{23}} + I_C \ln \frac{1}{D_{12}}\right] \tag{9}$$

$$\lambda_{A3} = 2 \times 10^{-7}\left[I_A \ln \frac{1}{D_{s3}} + I_B \ln \frac{1}{D_{31}} + I_C \ln \frac{1}{D_{23}}\right] \tag{10}$$

D_{s1} is GMR of bundle conductors located in position 1, and the same for D_{s2} and D_{s3}, since we are assuming the subconductor arrangements in three phases are not identical. In other words, for example, in the first transposition location, phase A which is initially located in position 1 is transposed to position 1, and its bundle arrangement changes to that in location 2. These bundle transpositions lead to having the same bundle arrangements in each location throughout the line. It should be noted that we have to do bundle arrangement transposition to meet, especially Eq. (1) obtained for a given location of subconductors in space.

Averaging the flux linkages, we have:

$$\lambda_A = \frac{\lambda_{A1} + \lambda_{A2} + \lambda_{A3}}{3} = \frac{2 \times 10^{-7}}{3} \left[I_A \ln \frac{1}{D_{s1} D_{s2} D_{s3}} + (I_B + I_C) \ln \frac{1}{D_{12} D_{23} D_{31}} \right] = \frac{2 \times 10^{-7}}{3} \left[I_A \ln \frac{1}{D_{s1} D_{s2} D_{s3}} + (-I_A) \ln \frac{1}{D_{12} D_{23} D_{31}} \right] = \frac{2 \times 10^{-7}}{3} I_A \left[\ln \frac{D_{12} D_{23} D_{31}}{D_{s1} D_{s2} D_{s3}} \right] = 2 \times 10^{-7} I_A \left[\ln \frac{\sqrt[3]{D_{12} D_{23} D_{31}}}{\sqrt[3]{D_{s1} D_{s2} D_{s3}}} \right] \quad (11)$$

from which, the average inductance of phase A is:

$$L_A = 2 \times 10^{-7} \left[\ln \frac{\sqrt[3]{D_{12} D_{23} D_{31}}}{\sqrt[3]{D_{s1} D_{s2} D_{s3}}} \right] \quad (12)$$

L_B and L_C are the same as L_A. In the above equations,

$$D_{12} = \left(\prod_{i=1}^{N} \prod_{j=1}^{N} D_{iA,jB} \right)^{1/N^2} \quad (13)$$

$$D_{13} = \left(\prod_{i=1}^{N} \prod_{j=1}^{N} D_{iA,jC} \right)^{1/N^2} \quad (14)$$

where $D_{iA,jB}$ is the distance from the i^{th} subconductor in phase A and the j^{th} subconductor in phase B, in the first $l/3$ length of the line, and the same approach for $D_{iA,jC}$. D_{s1} is found using:

$$D_{s1} = \left(\prod_{i=1}^{N} \prod_{j=1}^{N} D_{iA,jA} \right)^{1/N^2} \quad (15)$$

where $D_{iA,jA}$ is the distance from the i^{th} subconductor in phase A and the j^{th} subconductor in phase A, in the first $l/3$ length of the line, and $D_{1A,1A}$ is equal to conductor GMR. D_{s2} and D_{s3} for phases B and C can be obtained in the same way.

Capacitance, C, of unconventional HSIL lines can be found using:

$$C = \frac{2\pi \times 8.854 \times 10^{-12}}{\ln \frac{\sqrt[3]{D_{12} D_{23} D_{31}}}{\sqrt[3]{D_{sc1} D_{sc2} D_{sc3}}}} \quad (16)$$

where D_{sc1} is similar to D_{s1}, but, $D_{1a,1a}$ is equivalent to the outer radius of the conductor.

III. CASE STUDIES AND RESULTS

A. CONVENTIONAL LINES

An existing conventional line with the phases placed in a horizontal configuration is chosen as the base case of our study. Additionally, compact conventional lines in both horizontal and delta/inverted delta arrangements are designed for each considered value of N for comparison. The delta configurations are designed by considering the outer phase locations on hypothetical arcs having radii of 6.7 m and centered at the middle phase. The arcs represent the candidate locations of the outer phases.

Fig. 3 shows the conventional 500 kV Chang-An line with horizontal configuration and $N = 4$ [14]. Each of these subconductors has a diameter of 26.82 mm, a bundle spacing of 0.45 m, and the distance between the individual phases is 12.3 m with the centers of the phases being 28 m above the ground surface. Figs. 4 and 5 show the conventional lines designed in this paper with the highest SIL amongst the candidate designs. A comparative analysis of the conventional lines is drawn in Table 2.

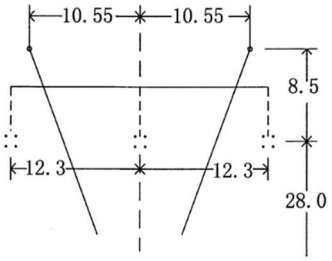

FIGURE 3. Line configuration of the existing 500 kV conventional line [14].

The designed horizontal configurations for each value of N were made as compact as possible while maintaining all the constraints to ensure the highest possible SIL to be gained at each level, i.e., making these line designs the optimal solutions. For each delta configuration, its mirror image about a horizontal axis drawn through the central phase gives an inverted delta configuration with the same natural power. The change in the SIL and E_{max} vs the height of the outer phases is demonstrated for each N value in Fig. 6.

It can be seen that for $N = 2$, the traditional horizontal configuration is designed in two ways, one of which has the subconductors in the two conductor bundles arranged horizontally (Fig. 4a), as well as vertically (Fig. 4b). For the latter, as the *GMD* is lower, whereas *GMR* remains constant, Z_c reduces and, in turn, leads to a slightly higher SIL value for Fig. 4b.

From Table 2, it can be observed that the natural power of the conventional configurations with $N \geq 3$ easily exceeds that of the existing 500 kV Chang-An line. The line width is reduced to much lower values for the newly designed horizontal conventional lines. In the delta configurations, the line width was lowered further, besides achieving higher SIL, resulting in the power density of these lines being much higher than other desirable new configurations.

To study the triangular, i.e., the delta and the inverted delta configurations, first, the central phase was fixed in position at a height of 28 m following the height of the phases of the conventional line shown in Fig. 3. Next, hypothetical arcs with radius 6.7 m were taken centered on the middle phase giving the candidate locations of the outer phases having position vector $Z = re^{i\theta}$, where r is the radius and θ is an angle parameter covering the arcs from $-\pi/2$ to $\pi/2$. Based

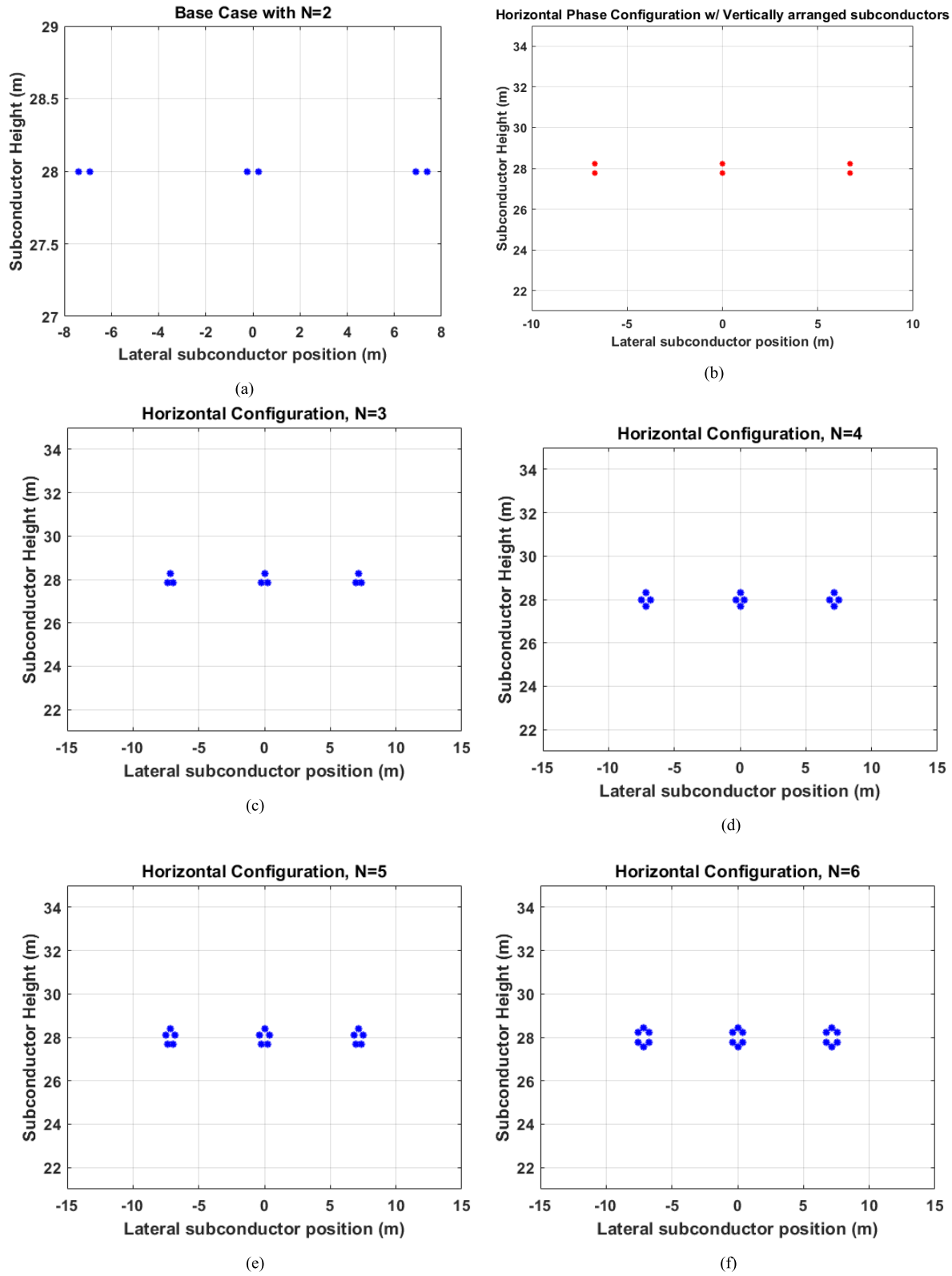

FIGURE 4. 500 kV horizontal conventional lines with (a) $N = 2$ (Type 1), (b) $N = 2$ (Type 2), (c) $N = 3$, (d) $N = 4$, (e) $N = 5$, and (f) $N = 6$.

on the constraint that keeps the interphase distance greater than 6.7 m, the candidate designs were found, and the ones with the highest SIL are the optimum designs.

It is understood that as the outer phases move from the horizontal configuration to form delta/inverted delta ones, the effective distance between the outer phases is reduced, i.e.,

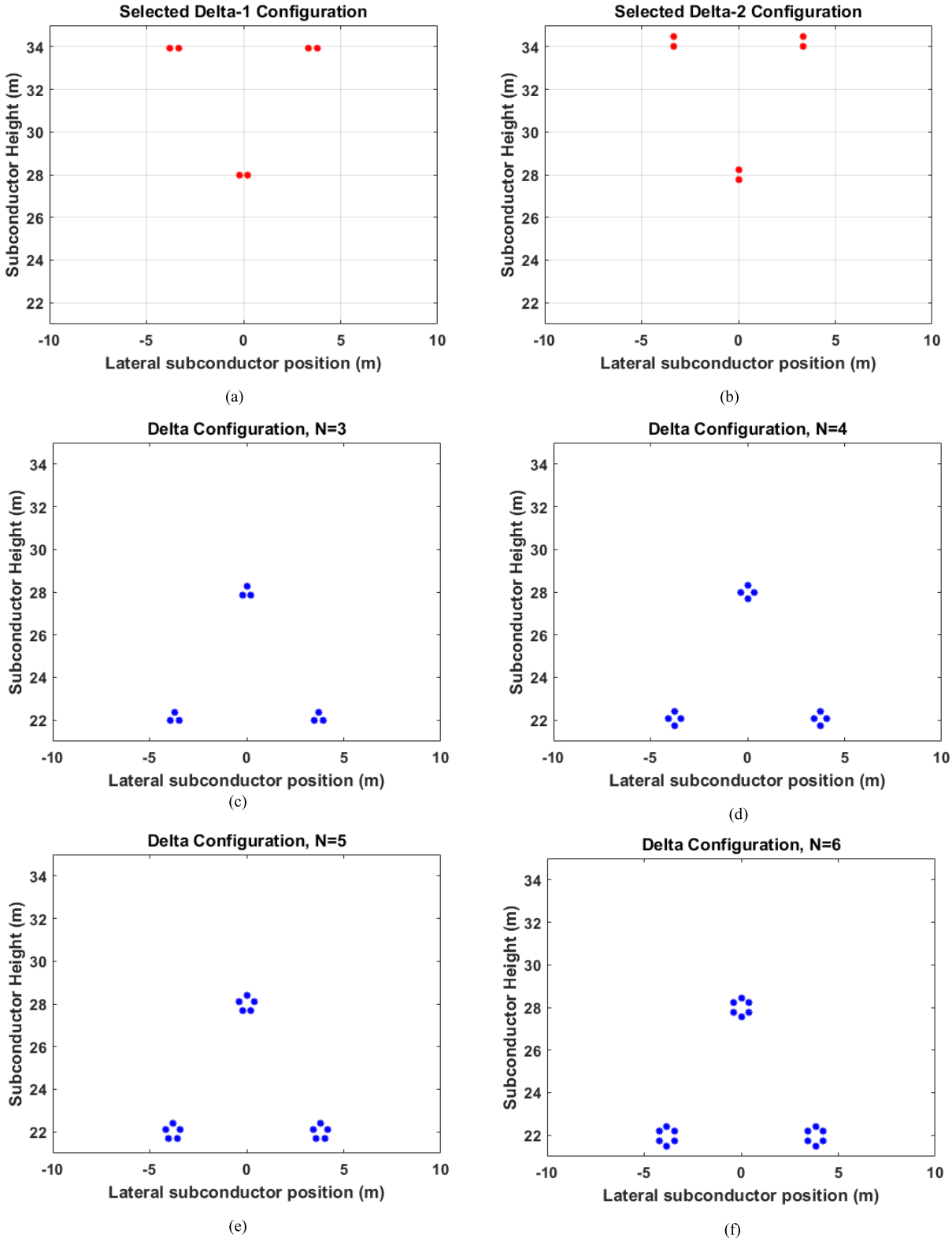

FIGURE 5. 500 kV conventional lines with triangular (delta/inverted delta) configuration having (a)) $N = 2$ (Type 1), (b) $N = 2$ (Type 2), (c) $N = 3$, (d) $N = 4$, (e) $N = 5$, and (f) $N = 6$.

a reduction in *GMD* occurs, while the *GMR* stays constant. This affects the surge impedance, taking it to lower values, and increasing the SIL.

B. UNCONVENTIONAL HSIL LINES

Traditionally, unconventional lines have been designed following evolutionary algorithms (EAs) as seen in [24], direct

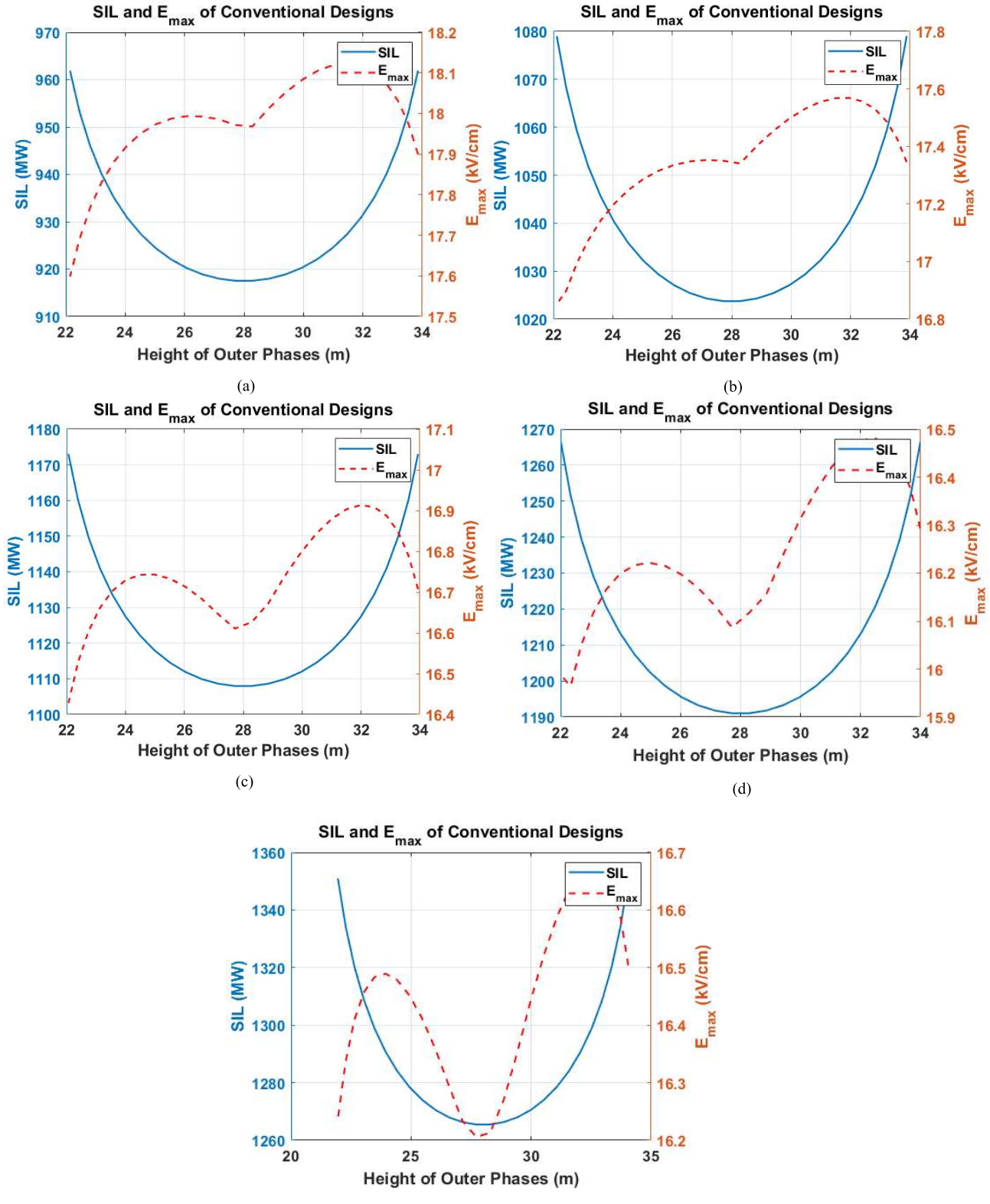

FIGURE 6. Change in E_{max} and SIL against the height of the outer phases for the conventional lines having (a) $N = 2$, (b) $N = 3$, (c) $N = 4$, (d) $N = 5$, and (e) $N = 6$.

search algorithms as seen in [7], etc. Evolutionary algorithms are a type of population-based optimization algorithm which takes its inspiration from natural evolution. Here, a random population of candidate solutions is chosen from which individual ones are selected based on the objective function. After that, these solutions are combined to form new candidates

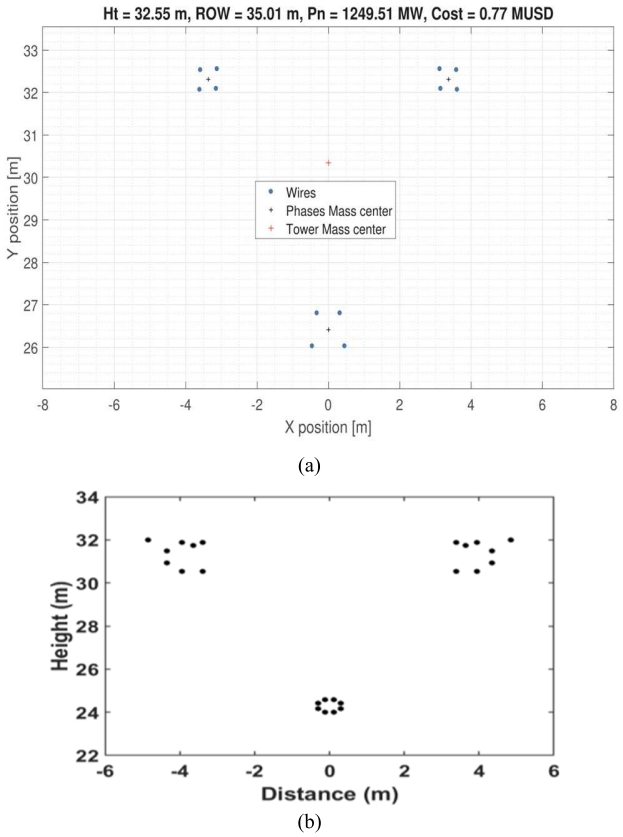

FIGURE 7. Unconventional line designs found in recent literature (a) $N = 4$ [24], and (c) $N = 8$ [7].

TABLE 2. Comparison of the conventional lines.

	Configuration	N	SIL (MW)	Corridor Width (m)
Conventional (Fig. 4a)	Horizontal-1	2	911.3	14.771
Conventional (Fig. 4b)	Horizontal-2	2	924.3	13.4
Conventional (Fig. 4c)	Horizontal	3	1016.8	14.771
Conventional (Fig. 4d)	Horizontal	4	1094.8	15.35
Conventional (Fig. 4e)	Horizontal	5	1187.7	15.05
Conventional (Fig. 4f)	Horizontal	6	1265.4	15.105
Conventional (Fig. 5a)	Inverted Delta-1	2	964.35	7.626
Conventional (Fig. 5b)	Inverted Delta-2	2	965.67	6.7
Conventional (Fig. 5c)	Delta	3	1079.0	7.9
Conventional (Fig. 5d)	Delta	4	1173.5	7.47
Conventional (Fig. 5e)	Delta	5	1266.5	8.317
Conventional (Fig. 5f)	Delta	6	1351.0	8.442
Conventional 500 kV Chang-An Line (Fig. 3)	Horizontal	4	996	24.6

TABLE 3. Comparison of the designed unconventional HSIL lines.

Configuration	N	SIL (MW)	Corridor Width (m)
Unconventional (Fig. 7a)	4	1249.5	-
Unconventional (Fig. 7b)	8	1414.7	9.70
Unconventional (Fig. 8a)	2	1137.9	13.857
Unconventional (Fig. 8b)	3	1303.6	13.857
Unconventional (Fig. 8c)	4	1414.2	18.85
Unconventional (Fig. 8d)	5	1475.8	13.61
Unconventional (Fig. 8e)	6	1592.2	13.53

which are used to fill the population, and this is repeated for several generations until the best output is returned. Direct search algorithms, on the other hand, work by searching for points that improve the objective functions from a set of trial points. The approach used for our work is close to direct search, where the set of points is chosen ensuring a minimum distance of 6.7 m between subconductors of each phase. Figs. 7a and 7b show unconventional transmission line designs found using EA and direct search algorithms respectively [7], [24].

The unconventional lines were designed such that the *GMR* could be effectively increased while keeping the *GMD* as low as possible because this would result in lower characteristic impedances, and thus, a higher natural power. To make the algorithm fast, we reduced the candidate search grid by considering the positions of the outer phase subconductors to be only on hypothetical arcs centered on fixed subconductors in the outer phases, instead of considering a rectangular grid. The radii of the arcs were increased starting from the bundle spacing of the conventional line of 0.457 m. For $N = 2$, this value was increased to go as much as 5.45 m, exceeding which caused the constraint surrounding the maximum conductor surface electric field to be violated. For $N = 3$ and $N = 4$, the corresponding maximum radii of the hypothetical arcs are 2.65 m and 2.40 m, respectively. However, changing the design from $N = 3$ to $N = 4$ required the corridor width to be increased by 36%. Adding more conductors the same way would mean a further increase in the width. Thus, for $N = 5$ and $N = 6$, we slightly changed our approach. For the five subconductor design, we split the outer phase conductors into two segments, one consisting of two and the other containing the remaining three. To ensure the constraint in (2) is satisfied, we then calculated the bundle radius, R for the central phase and added 6.7 m which was the $D_{min,p2p}$ considered for this work. This value was chosen as the radius of the arcs about the center of the middle phase – which means, all the outer subconductors lying in these arcs would meet (2). The positions of the outer phase segments were then varied along these two arcs to find the design that showed the highest *SIL* while also complying with (1). Similarly, the configuration for $N = 6$ was found. The only change here is that each segment now contains three subconductors. Table 3 demonstrates the unconventional line details, where it can be seen that for increasing N, the *SIL* increases, and its highest value is obtained under the $N = 6$ condition. The changed approach also enables a way to keep the corridor width low for $N = 5$ and beyond.

Fig. 8 shows the optimally designed high natural power unconventional lines. As seen in Fig. 8, each of the

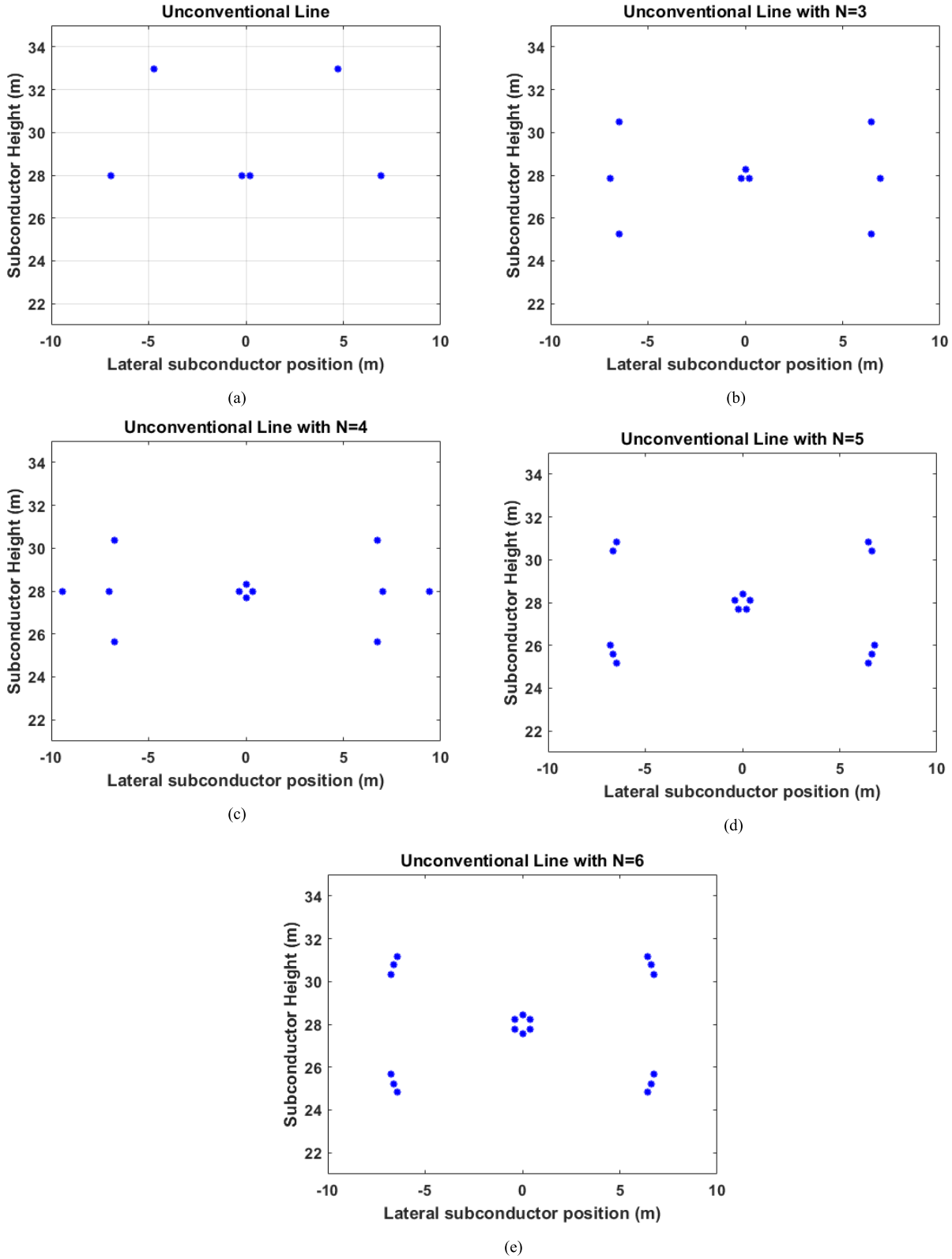

FIGURE 8. New Unconventional line designs with (a) $N = 2$, (b) $N = 3$, (c) $N = 4$, (d) $N = 5$, and (e) $N = 6$.

designed unconventional lines has outer phases with large distances between subconductors in each phase, causing an increase in the line's *GMR*, and in turn a reduction in the line inductance and an increase in the line capacitance.

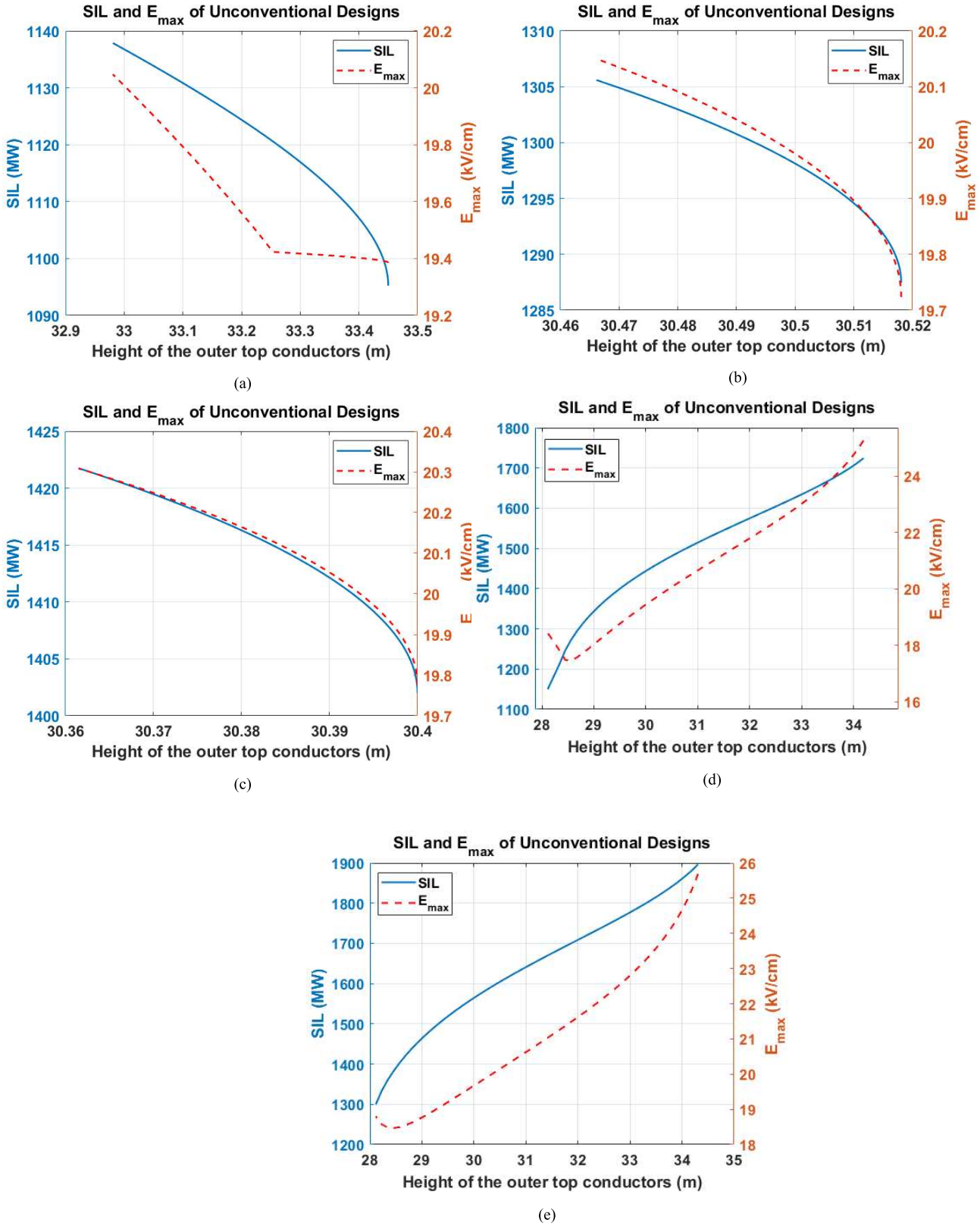

FIGURE 9. Change in E_{max} and SIL against the height of the outer phases for the unconventional lines having (a) $N = 2$, (b) $N = 3$, (c) $N = 4$, (d) $N = 5$, and (e) $N = 6$.

Each of the unconventional designs exceeds the natural power of the conventional line shown in Fig. 3, and the line shown in Fig. 8e exceeds the SIL of all the unconventional HSIL line designs presented in this

paper, Figs. 8a to 8d, and those demonstrated in [7] and [24].

Fig. 9 shows the variation in SIL and E_{max} with the height of the uppermost subconductors of the outer phases. As the design approach is changed for $N = 5$ and 6, it can be seen that, for the increased height of the outer top subconductors, the *SIL* increases, and so does E_i^{max}, which is different for the designs with lower N. This paper presents a comprehensive combination of results obtained from different designs with different numbers of subconductors in the bundle. As the unconventional design configurations have increased *GMR* and reduced *GMD* compared to the base design, a higher *SIL* or power capacity is naturally obtained. It is also seen that increasing N also increases the *SIL*, while having no visual increase in conductor costs. However, for $N = 4$, the corridor width is higher compared to the other unconventional designs, but still lower than that of the base design making it yet another improvement.

IV. CONCLUSION

In this paper, new transmission lines with conventional and unconventional configurations designed optimally were presented. The proposed lines not only show the potential to transmit higher power but also cover a much lower line width compared to an existing 500 kV conventional transmission line. Specifically, we see that the conventional horizontal configuration lines with $N = 2$ and $N = 3$ exceed the power density of the base case by 70% and for $N = 4$, 5, and 6, this number is 76%, 94%, and 107% respectively. The delta configurations on the other hand show a massive rise in power density compared to the horizontal ones, as the above values become 256%, 237%, 288%, 276%, and 297% respectively for the new delta configurations. For the unconventional lines, the increases in SIL are significantly higher. For $N = 2$, there is a 14.2% increase in SIL while the line width reduces by 43.7%. For $N = 3$, the SIL increases by 30.9% while the line width reduces by the same amount. For $N = 4$, 5, and 6, the increases in SIL are as high as 42.0%, 48.2%, and 59.8%, with a reduction in line width by 23.4%, 44.7%, and 45% respectively compared to the existing conventional line. The $N = 6$ design also showed a 27.4% and 12.5% increase in SIL compared to previous unconventional line designs from literature. The proposed lines can have the potential to play a critical role in future modern transmission networks. As challenges and future work, maintaining the positions of the subconductors can be one of the practical challenges that might be faced during practical implementation of such unconventional lines. Typical spacer sizes for EHV lines are around 18 in or 0.4572 m, which is much lower than the distances between the subconductors of the proposed designs [24]. However, this also opens up the possibility of designing new bundle spacers. While our current research is based on unconventional line designs for EHV levels as shown above, our future research encompasses working with lower voltage levels, such as 230 and 345 kV. In [25], we find some work done on multi-circuit transmission lines above the 230 kV level which fits with the definition of unconventional lines. In the future, we will attempt to design unconventional HSIL lines for double-circuit configurations as well.

REFERENCES

[1] M. Ghassemi, "High surge impedance loading (HSIL) lines: A review identifying opportunities, challenges, and future research needs," *IEEE Trans. Power Del.*, vol. 34, no. 5, pp. 1909–1924, Oct. 2019.

[2] E. Larson, "Net-zero America: Potential pathways, infrastructure, and impacts," Princeton Univ., Princeton, NJ, USA, Tech. Rep., 2020. [Online]. Available: https://netzeroamerica.princeton.edu/img/Princeton_NZA_Interim_Report_15_Dec_2020_FINAL.pdf

[3] (May 1, 2024). *MISO Transmission Cost Estimation Guide for MTEP24*. [Online]. Available: https://cdn.misoenergy.org/MISO%20Transmission%20Cost%20Estimation%20Guide%20for%20MTEP24337433.pdf

[4] B. Dhamala and M. Ghassemi, "Transmission expansion planning with high surge impedance loading lines at reduced voltage levels," *J. Mod. Power Syst. Clean Energy*, early access, Mar. 27, 2025, doi: 10.35833/MPCE.2024.001149.

[5] B. Dhamala and M. Ghassemi, "Smart transmission expansion planning based on the system requirements: A comparative study with unconventional lines," *Energies*, vol. 17, no. 8, p. 1912, Apr. 2024.

[6] B. Dhamala and M. Ghassemi, "Comparative study of transmission expansion planning with conventional and unconventional high surge impedance loading (HSIL) lines," in *Proc. IEEE Power Energy Soc. Gen. Meeting (PESGM)*, Jul. 2024, pp. 1–5.

[7] M. Abedin Khan, E. Arafat, S. Chowdhury, and M. Ghassemi, "Optimally located subconductors and phases to achieve transmission lines with high natural power and narrow corridor width," *IEEE Access*, vol. 13, pp. 7338–7352, 2025.

[8] G. N. Alexandrov, "Design of compacted UHV transmission line," Energoatomizdat, Moscow, Russia, Tech. Rep., 1993.

[9] G. N. Alexandrov and G. V. Podporkyn, "Improvement of the efficiency of 35 to 220 kV lines," in *Proc. Int. Conf. AC DC Power Transmiss.*, London, U.K., Sep. 1991, pp. 226–231.

[10] G. N. Alexandrov, "Electrical power transmission," St. Petersburg Polytechnic Univ., St. Petersburg, Russia, Tech. Rep., 2009.

[11] G. N. Alexandrov, V. P. Dikoi, S. V. Krylov, O. A. Nikitin, and L. V. Timashova, "Overhead line designing in view of environmental constraints compact overhead lines," in *Proc. CIGRE*, Paris, France, 1998.

[12] R. G. Olsen and C. Zhuang, "The spatial distribution of electric field as a unifying idea in transmission line design," *IEEE Trans. Power Del.*, vol. 34, no. 3, pp. 919–928, Jun. 2019.

[13] *BOLD*. Accessed: Apr. 20, 2025. [Online]. Available: https://www.boldtransmission.com/

[14] H. Wei-Gang, "Study on conductor configuration of 500-kV Chang-Fang compact line," *IEEE Trans. Power Del.*, vol. 18, no. 3, pp. 1002–1008, Jul. 2003.

[15] J. H. M. Fernandes et al., "500 kV compact line of eletronorte Brazil-conception, electrical and mechanical design," in *Proc. CIGRE*, Paris, France, 1990.

[16] O. Regis, S. J. C. Gusmao, A. N. Pessoa, F. C. Dart, L. A. C. Domingues, and M. J. A. Maia, "Expanded bundle technique: The application of HSIL TL concept to increase the capacity of overhead lines," in *Proc. CIGRE*, Paris, France, 1998.

[17] F. C. Dart, C. K. C. Arruda, R. W. Garcia, and O. Regis, "High capacity AC transmission lines—The Brazilian experience," in *Proc. CIGRE/IEC Symp.*, Cape Town, South Africa, 2015.

[18] P. C. V. Esmeraldo, C. P. R. Gabaglia, G. N. Aleksandrov, I. A. Gerasimov, and G. N. Evdokunin, "A proposed design for the new FURNAS 500 kV transmission lines—The high surge impedance loading line," *IEEE Trans. Power Del.*, vol. 14, no. 1, pp. 278–286, Jan. 1999.

[19] O. Regis, "Increasing the transmission capacity of overhead lines-high surge impedance loading technique," *Electra*, no. 221, Aug. 2005.

[20] W. Watson, "Extra high voltage AC transmission engineering," *Electron. Power*, vol. 33, no. 1, pp. 70, Jan. 1987.
[21] PAR Electrical Contractors Inc. *Experience With 345 KV and 500 KV Line*. Accessed: Apr. 20, 2025. [Online]. Available: https://www.efis.psc.mo.gov/Document/Display/292118
[22] *General Cable Datasheet, Electric Utility*, U.S. Energy Products for Power Generation, Transmission & Distribution, Highland Heights, KY, USA, May 2017.
[23] M. A. Khan and M. Ghassemi, "A new method for calculating electric field intensity on subconductors in unconventional high voltage, high power density transmission lines," in *Proc. IEEE Conf. Electr. Insul. Dielectr. Phenomena (CEIDP)*, Oct. 2023, pp. 1–4.
[24] *Transmission Line Reference Book −345 KV and Above*, Electric Power Research Institute, Palo Alto, CA, USA, 1982.
[25] J. S. Acosta and M. C. Tavares, "Optimal selection and positioning of conductors in multi-circuit overhead transmission lines using evolutionary computing," *Electr. Power Syst. Res.*, vol. 180, Mar. 2020, Art. no. 106174.

MUSHFIQUL ABEDIN KHAN (Graduate Student Member, IEEE) received the B.S. degree from Bangladesh University of Engineering and Technology (BUET), Bangladesh. He is currently pursuing the Ph.D. degree in electrical engineering with The University of Texas at Dallas, TX, USA. His research interests include optimization, transmission line design, unconventional line design, corona discharge, applications of machine learning, and signal processing.

MONA GHASSEMI (Senior Member, IEEE) received the Ph.D. degree (Hons.) in electrical engineering from the University of Tehran, Tehran, in 2012.

From 2013 to 2015, she was a Postdoctoral Fellow with NSERC/Hydro-Québec/UQAC Industrial Chair on Atmospheric Icing of Power Network Equipment (CIGELE), University of Québec at Chicoutimi (UQAC), Chicoutimi, QC, Canada. She has been a Registered Professional Engineer, since 2015. She was also a Postdoctoral Fellow with the University of Connecticut, Storrs, CT, USA, from 2015 to 2017. In 2017, she joined the Bradley Department of Electrical and Computer Engineering, Virginia Tech, Blacksburg, VA, USA, as an Assistant Professor. In 2021, she was named both the Steven O. Lane Junior Faculty Fellow and the College of Engineering Faculty Fellow of Virginia Tech. In 2022, she joined the Department of Electrical and Computer Engineering, The University of Texas at Dallas, as an Associate Professor, and the Chairholder of Texas Instruments Early Career Award, from 2022 to 2028. She has authored over 200 peer-reviewed journal and conference papers and one book chapter. Her research interests include electrical insulation materials and systems, high voltage/field engineering and technology, power systems, and plasma science. She was a member of the Nominations and Appointments Committee of the IEEE DEIS, an At-Large Member of the Administrative Committee of the IEEE DEIS, and a DEIS Representative of the IEEE USA Public Policy Committee on Transportation and Aerospace Policy (CTAP). She is an Active Member of several CIGRE working groups and the IEEE Task Forces, a DEIS Technical Committee Member on Dielectrics and Electrical Insulation for Transportation Electrification, and a member of the Education Committee of IEEE DEIS and Power and Energy Society (PES).She received the three most prestigious and most competitive career awards the Department of Energy (DOE) Early Career Research Program Award, the National Science Foundation (NSF) CAREER Award, and the Air Force Office of Scientific Research (AFOSR) Young Investigator Research Program (YIP) Award. She received the Contribution Award from *IET High Voltage*and four Best Paper awards. She is an Associate Editor of IEEE TRANSACTIONS ON DIELECTRICS AND ELECTRICAL INSULATION, IEEE TRANSACTIONS ON INDUSTRY APPLICATIONS, *IET High Voltage*, *International Journal of Electrical Engineering Education*, and *Power Electronic Devices and Components*, a Guest Editor of *Aerospace* and *Energies*, and an Associate Guest Editor of IEEE JOURNAL OF EMERGING AND SELECTED TOPICS IN POWER ELECTRONICS. She is the Vice-President (Technical) of the IEEE Dielectrics and Electrical Insulation Society (DEIS), a DEIS Representative of the IEEE USA Technology Policy Council Research and Development Policy Committee.